Microwave Instability at Transition Crossing: Experiments and a Proton-Klystron Model

Ken Takayama, Dai Arakawa, Junichi Kishiro, Kiyomi Koba, and Masahito Yoshii
National Laboratory for High Energy Physics in Japan (KEK), 1-1 Oho, Tsukuba, Ibaraki 305 Japan
(Received 16 September 1996)

Longitudinal bunch shapes in the KEK proton synchrotron were measured by a fast bunch-monitor system, which showed the rapid growth of the instability at the frequency of ~1 GHz and significant beam loss just after transition energy. Temporal evolution of the microwave instability is explained for the first time with a proton-klystron model. [S0031-9007(96)02288-0]

PACS numbers: 29.27.Bd

Transition crossing (TC) in a proton synchrotron (PS) is one of the classical issues in accelerator beam dynamics [1]. The transition energy (TE) is well known to be a singular point on the way of acceleration. At this point the synchrotron phase motion is completely frozen and bunch shape becomes inclined in the longitudinal phase space due to the *nonadiabatic* feature in TC. Asymmetric bunch stretching in the phase space caused by nonlinear kinematics effects (Johnsen effects [2]) becomes significant. Succeeding bunch shape mismatching beyond TC is inevitable due to *time irreversibility* of these nonlinear kinematics terms about rf phase jump [3]. Space-charge effects are also other sources of mismatching beyond the TE [4]. Another big issue at TC is the microwave instability (MI) caused by various interactive resonant structures along the beam path which was originally observed in CERN-ISR. The Boussard conjecture of the MI for the bunched beam has also been rigorously proved by broad-band impedance models [5]. Individual mechanisms of the MI in the vicinity of the TE driven by *capacitive*, *inductive*, and *resistive* impedances have been clearly delineated by Wei [6] in the broad-band impedance regime. The importance of the induced voltage in a higher frequency narrow-band resonant structure at TC which will be understood later to play a key role in the observed MI has been pointed out in Ref. [7]. To the authors' knowledge, however, there have been no reports of systematic experiments focusing on the MI at TC, while theoretical analyses to evaluate its particular features observed only at the TE are quite limited [6,8].

The KEK 12 GeV PS has been subjected to serious damage by the MI at TC since the beginning of its operation [9]. Since KEK PS's impedance budget has never been concerned, a lot of high impedance materials as discussed later are *periodically* located along the ring, following lattice components. The observed threshold beam current for the MI and size of Landau damping due to γ_t jump are different in order of magnitude from that of the theoretical estimation based on the existing broad-band model. In this Letter recent studies on the longitudinal impedance, extensive beam experiments of TC, and a proton-klystron model capable of consistently explaining the experimental results will be presented.

Experimental results.—Through the experiments a single bunch operation was employed to exclude coupled bunch-to-bunch interactions and any undesired ambiguity. A single bunch (500 MeV) from the booster ring was injected into the 12 GeV PS ring waiting with standing RF buckets of harmonic 9. The beam intensity ($1-5 \times 10^{11}$/bunch) was controlled by changing the H^- beam spill length hitting a stripping carbon foil in the booster and the longitudinal emittance was controlled by introducing a coherent rf-phase modulation in the 12 GeV ring [10] within 0.65–1.3 eV sec at transition ($\gamma = 6.63$), the rf frequency is ~7 MHz, and the synchronous phase is switched from 15° to 165°. To elucidate the dependence of the MI on phase-mixing speed, the size of γ_t jump, $\Delta\gamma_t$, was varied up to 0.25 for 0.5 msec. Longitudinal bunch information was a signal from the fast wall-current monitor with ~2 GHz resolution.

The MI observed in the KEK PS always grows from the tail portion [10]. Figure 1 shows a typical evolution of the bunch shape projected on the time axis. Below transition the MI never evolves to an observable level, just after TC it dramatically starts to grow within 1 msec near 1 GHz, then a fraction goes away from the bunch center. The latter suggests the lower edge of microstructures should get over the separatrics boundary. The surviving bunch core seems to still place in the rf bucket with an extremely large emittance and to be accelerated. High frequency (400 MHz–12 GHz) components of the beam-induced signal on the vertical plate in the beam position monitor (BPM) were obtained by a spectrum analyzer; the 1.23 GHz component is remarkable after TC when the instability occurs. Hence it turns out that this component is related to the MI and its frequency is in agreement with the modulation frequency observed in the bunch profile.

A threshold current for the MI was obtained by measuring the size of the emittance blow-up ratio (EBR) for different beam currents. The emittance was calculated from the bunch size in time assuming a matched rf bucket. The EBR here was defined as a ratio of the 10 msec down-stream emittance to 10 msec up-stream one; damping in the emittance associated with acceleration was ignored because it is negligibly small for this short time period. Figure 2 shows the ratio as a function of the particle number per bunch. Beyond some critical value of

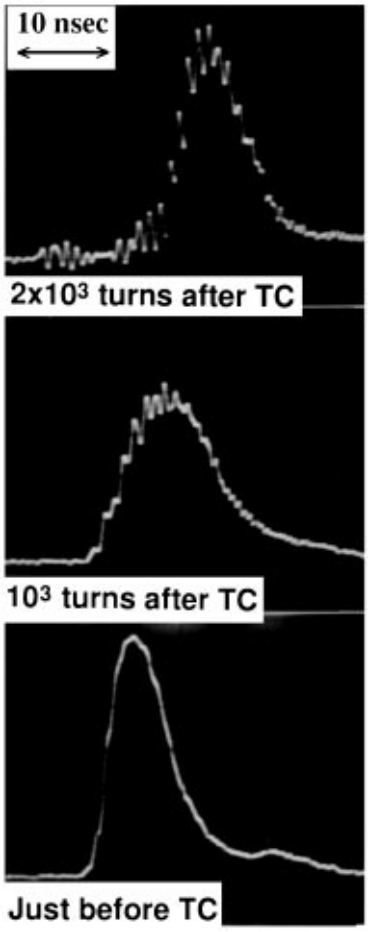

FIG. 1. Bunch profiles from −1 msec to +2 msec (t = 0 msec: transition).

particle number the blow up becomes obvious. The dependence of the EBR on a size of γ_t jump is depicted in Fig. 3 for a fixed beam current of $N = 5 \times 10^{11}$. Non linear kinematics effects are responsible for a change in the emittance under the condition of the small γ_t jump [3]; that is, $d\gamma_t/dt = 0{-}2 \times 10^2/\text{sec}$ where asymmetric bunch stretching and associated mismatching are significant. The synergism of both effects should be dominant in this region. The experimental results reflect the fact.

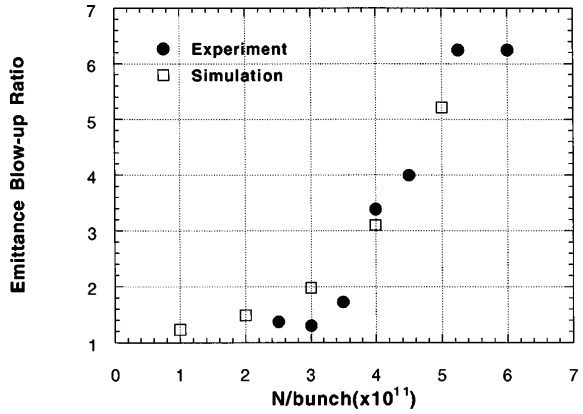

FIG. 2. Emittance blow-up ratio vs the number of particles.

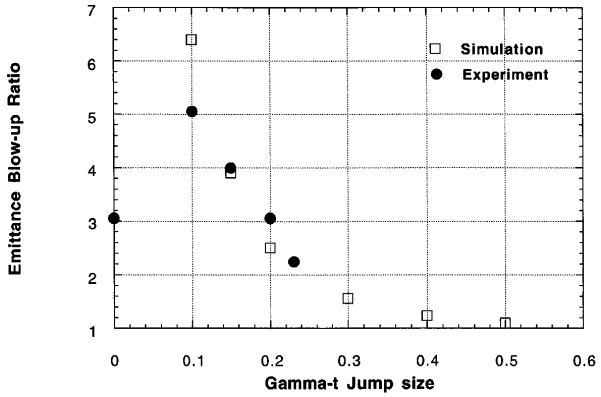

FIG. 3. Emittance blow-up ratio vs the size of γ_t jump ($\Delta\gamma_t$).

Resonant impedance calculations and measurements.—Resonant structures (RS) capable of exciting the observed MI have been identified as a result of MAFIA calculations and impedance measurements at the test bench. As shown in Table I, the BPM [11] and cavitylike vacuum chamber (CVC), which are placed at each side of every lattice quadrupole magnet, have a large shunt impedance R_{shunt} in the order of $10^4{-}10^5\ \Omega$ and a high quality factor Q of $10^2{-}10^3$ at the resonant frequency of 0.7−1.4 GHz. In the numerical simulations, a magnitude of R_{shunt}/Q obtained by the MAFIA calculations and measurements has been used, which are in agreement to each other in order of magnitude, while the quality factor was treated as a kind of free parameter because a loaded Q in the actual ring is not satisfactorily estimated.

Proton-klystron model (PKM).—In order to totally understand the experimental results, the PKM as schematically depicted in Fig. 4 was developed. In the model highly RS are periodically distributed along the beam path and wake fields excited by the bunch head can affect the bunch tail. Member change on a global scale between the bunch head and tail scarcely occurs near transition. The interaction between a proton bunch and RS is quite analogous to that in a klystron driven by electron beams. All excited RS can be regarded as idling cavities. Buildup of the wakes in each RS is treated in a formulation of the forced excitation of a damped harmonic oscillator [12].

Turn-by-turn longitudinal motio

n of a particle is governed by a set of discrete kinetic equations for energy E and phase ϕ to the accelerating rf

TABLE I. Resonant impedance (measurement/calculation).

	$\omega_\lambda/2\pi$ (GHz)	Q	R_{shunt} (Ω)	R/Q (Ω)
BPM	0.636/0.667	77/2650	$1.5 \times 10^3/2.6 \times 10^4$	19.4/9.8
	/1.13	/3769	$/6.2 \times 10^4$	/16.3
	1.498/1.377	230/8222	$5.3 \times 10^3/3.3 \times 10^5$	23/40
CVC	/1.44	/4846	$/1.39 \times 10^5$	/28.8
	/1.84	/4078	$/1.94 \times 10^5$	/46.6

excited at $\omega_{\rm rf}$, taking into account normal rf acceleration, longitudinal space-charge forces, and interactions with the RS,

$$E^{n+1} = E^n + eV\sin(\phi^n) + \frac{ce\pi Z_0 g_0 h^2}{C_0\gamma_s^2}\frac{\partial\lambda(\phi)}{\partial\phi} + eV_{\rm int}(\phi), \quad (1)$$

$$\phi^{n+1} = \phi^n + 2\pi h\left[(\alpha_0 - 1/\gamma_s^2)\delta + \left(\alpha_1 + \frac{3\beta_s^2}{2\gamma_s^2}\right)\delta^2\right] + \Delta\phi_{s,n+1}, \quad \left(\delta \equiv \frac{E^{n+1} - E_s^{n+1}}{\beta_s^2 E_s^{n+1}}\right), \quad (2)$$

where the quadratic term of δ denotes nonlinear kinematics effects mentioned earlier, $\Delta\phi_s$ is the variation per turn of ϕ_s and $eV_{\rm int}(\phi)$ represents a net change in energy given by the wakes in the RS, which is described by

$$V_{\rm int}(\phi) = M\frac{2e\omega_{\rm rf}}{TTF}\left(\frac{R_{\rm shunt}}{Q}\right)\int_{\phi_{\rm head}}^{\phi}\exp\left(-\frac{\omega_\lambda(\phi - \phi')}{2Q\omega_{\rm rf}}\right) \times \sin\left(\frac{\omega'_\lambda}{\omega_{\rm rf}}(\phi' - \phi)\right)\frac{\partial\lambda(\phi')}{\partial\phi'}\,d\phi'. \quad (3)$$

In Eqs. (1), (2), and (3) e is the unit charge, V is the integrated accelerating voltage of 92 kV, c is the velocity of light, Z_0 is the impedance of vacuum (377 Ω), the geometric factor $g_0 = 1 + 2\ln(b/a)$ (a,b: averaged beam/chamber radius, 1.5 cm/5.5 cm), h is the harmonic number, C_0 is the ring circumference of 340 m, E_s, γ_s, and β_s are the energy, relativistic gamma, and normalized velocity of the synchronous particle, respectively, $\lambda(\phi)$ is the beam line density, α_0 and α_1 are the linear and second-order momentum compaction factors, respectively [3,6], *TTF* is the transit-time factor of the RS, ω_λ, and ω'_λ $(=\omega_\lambda/R[1 - (1//2Q^2)] \approx \omega_\lambda)$ are the angular frequency of the RS, and M is the number of the RS, 56. The integration form is essentially identical to the usual form written in the term of the longitudinal wake function $W'(\phi)$ [5], $\propto\int_{\phi_{\rm head}}^{\phi} W'(\phi - \phi')I_0(\phi')\,d\phi'$ where the impedance is fully resistive. Here we assume that member change over adjacent microstructures in a bunch does not occur in one turn because of the almost frozen phase motion and the RS are excited in the same manner at least in one turn. The wake's effects at M structures are simply superimposed. α_0 and α_1 are functions of time because the γ_t-jump scheme is employed here.

Simulation results.—Using a set of typical parameters close to that in the experiments, the temporal evolution of a bunch was numerically obtained by tracking based on Eqs. (1) and (2). The experimental complexity to determine the size of α_1 dictates calculation using the lattice parameters taking into accounts of sextupole fields. Appropriate smoothing in the line density, the number of macroparticles (10^6), and binning width of $2\pi/6000$ have been taken as a result of a compromise between numerical accuracy and computational speed (30 cpu h/run on DEC 3000 AXP-500). As seen in Figs. 5(a)–5(c) the simulation reproduces the essential aspects of the experimental result: (1) no notable growth of the MI below TE, (2) its rapid growth just after the TC, (3) run away of a bunch fraction, and (4) large blow up of the emittance after the TC process.

General features of the MI are (a) efficient energy transfer from beam to microwaves results from the deceleration of the microstructure's core, yielding the drift of the cores in the negative direction of the momentum space, (b) the interaction between wakes and the beam tends to occur in the bunch tail due to the finite Q value, and (c) the convection of the microstructure formation toward the bunch head is crucial for the same reason as that of (b). According to (b) and (c), the particles located in the region of $E > E_s$ and $\phi > \phi_s$ below the

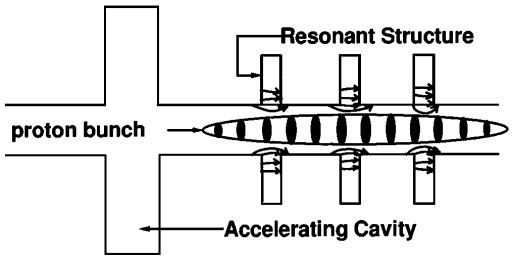

FIG. 4. Schematic view of the proton-klystron model.

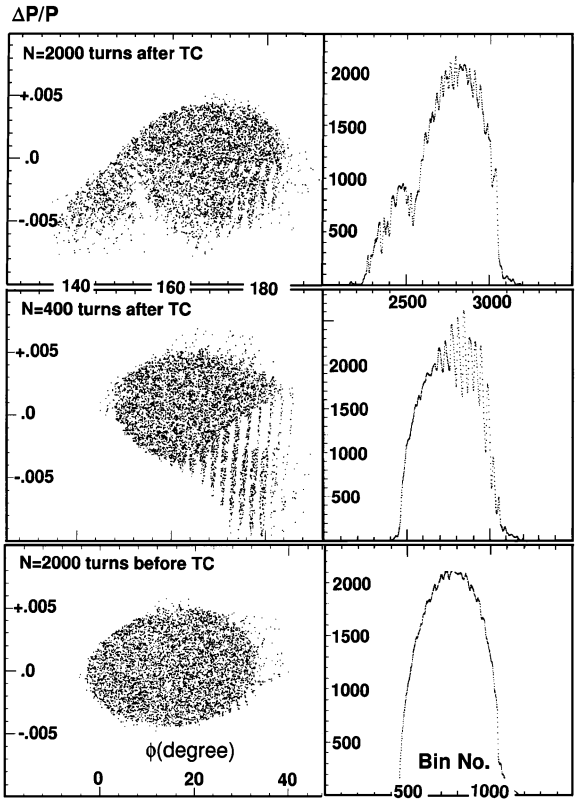

FIG. 5. (a)–(c) Typical simulation results of TC.

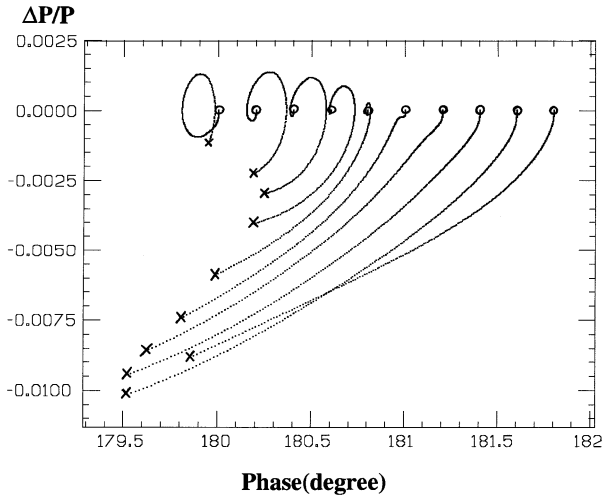

FIG. 6. Phase motion of test particles in the microbucket in the early stage just after TC (≤400 turns). The bucket extends over ±1 deg on the phase axis. Circles and crosses represent the initial positions and positions after 400 turns, respectively.

TE and $E < E_s$ and $\phi > \phi_s$ above the TE can contribute to the evolution of the MI. Since the wake's phase coincides with the motion of the microstructure's core, the particles located on the other side of momentum space are affected by the wake in counter phase, suffering a fast modulation in their motion. Below the TE a fraction of decelerated microbunch core necessarily falls into the region of $E < E_s$ where the fraction is forced to move in the opposite direction of the phase ϕ; the microbunch formation is likely to be wiped out. Thus the MI is not able to evolve to a level comparable to that above the TE.

In the early stage (≤400 turns) bunching and amplification proceed like that in a microwave amplifier such as free-electron lasers; the repeated synchrotron rotation in the microbucket does not occur but particles almost drift in the momentum space. Their behaviors depend on their initial conditions just at transition as seen in Fig. 6. A fraction of the microstructure placed in the decelerating phase is rapidly decelerated, amplifying the microwaves. The microwaves' phase follows the motion of the decelerated fraction because electromagnetic waves are amplified at the expense of the kinetic energy of protons. Consequently even the other fraction having been placed in the accelerating phase falls into the decelerating phase to turn to contribute to further microstructure formation. This looks like eruption in the bunch tail [see Fig. 5(b)].

Simulation results indicated that for the fixed value of $R_{\rm shunt}/Q = 10\ \Omega$ and $(\Delta\gamma_t) = 0.15$ the bunch eruption due to the MI is remarkable beyond $N_0 = 3 \times 10^{11}$ as seen in Fig. 2. From the expression of wake effects Eq. (3), the product of $R_{\rm shunt}/Q$ and N_0 is considered to be a sort of parameter to determine the evolution of MI; in the present case $(R_{\rm shunt}/Q)N_0 = 3 \times 10^{12}\ \Omega$ where it becomes critical. Simulations showed larger suppression of the MI as the size of $d\gamma_t/dt$ $[=2(\Delta\gamma_t)_{\rm max}/\Delta t]$ increases (see Fig. 3) and are in good agreement with the experimental results. The fast phase mixing in a case of the large $(\Delta\gamma_t)_{\rm max}$ is likely to prevent the MI from growing up. There is a notable difference in the region of small size of $d\gamma_t/dt$ where the nonlinear kinematics effects are dominant and a beam bunch asymmetrically stretches in the direction of $\Delta p/p > 0$. There the momentum spread in the bunch tail exceeds the momentum aperture; accordingly a significant fraction of the bunch tail is lost. The impedance measurement and MAFIA simulations indicate that plural resonant modes can be excited in the identified structures with different frequency and the similar magnitude of shunt impedance. In order to evaluate interference among different frequency modes, multifrequency simulations were performed where 1.14 GHz and 700 MHz resonant modes were included in the calculation. The mode with a large growth rate simply evolved. To confirm the relative importance of the broad-band space-charge impedance in the present MI, space-charge forces in Eq. (1) were turned off; there any notable change in the eruptionlike feature was not found.

In conclusion, the systematic experimental results of the MI at TC were presented for the first time. Their particular aspects of eruptionlike breakup just after TC and its evolution from the tail half, which have never been anticipated by the conventional collective instability theory and simulation where a cumulative feature of the beam-cavity interaction in a finite time period is not taken into account, were clearly manifested by the PKM.

The authors thank I. Yamane, S. Ninomiya, and other KEK-PS members for their interest and continual support through this work. One of authors (K. T.) acknowledges S. Y. Lee and J. Wei for useful discussions and comments.

[1] E. D. Courant and H. S. Snyder, Ann. Phys. (N.Y.) **3**, 1 (1958).
[2] K. Johnsen, in *Proceedings of the CERN Symposium on the High Energy Accelerators* (CERN, Geneva, Switzerland, 1956), Vol. 1, p. 44.
[3] K. Takayama, Part. Accel. **14**, 201 (1984).
[4] W. W. Lee and L. C. Teng, Fermilab Report No. FN-223, 1971; A. Sørenssen, Part. Accel. **6**, 141 (1975).
[5] A. W. Chao, *Physics of Collective Beam Instabilities in High Energy Accelerators* (John Wiley & Sons, Inc., New York, 1993), p. 84, and references therein.
[6] J. Wei, Ph.D. thesis 1990.
[7] S. Y. Lee and J. Wei, in *Proceedings of the 1989 IEEE Particle Accelerator Conference* (IEEE, New York, 1989), p. 1169.
[8] S. Y. Lee and J. M. Wang, IEEE Trans. Nucl. Sci. **32**, 2323 (1985).
[9] Y. Mizumachi and K. Muto, IEEE Trans. Nucl. Sci. **28**, 2563 (1981); T. Ieiri (private communication).
[10] S. Ninomiya (private communication).
[11] K. Satoh, Rev. Sci. Instrum. **50**, 450 (1979).
[12] E. U. Condon, J. Appl. Phys. **12**, 129 (1941).